Development and experimental validation of a multidirectional circular wave basin using smoothed particle hydrodynamics

RESEARCH PAPER

Development and Experimental Validation of a Multidirectional Circular Wave Basin using Smoothed Particle Hydrodynamics

Taiga Kanehira[a], Hidemi Mutsuda[b], Yasuaki Doi[b], Naokazu Taniguchi[b], Samuel Draycott[c] and David Ingram[c]

[a] Transportation and Environmental Systems, Graduate School of Engineering, Hiroshima University, Japan; [b] Academy of Science and Technology, Mechanical Engineering/Integrated Engineering Unit, Graduate School of Engineering, Hiroshima University, Japan; [c] School of Engineering, Institute for Energy Systems, The University of Edinburgh, Edinburgh, U.K.

ARTICLE HISTORY
Compiled January 22, 2019

ABSTRACT

Several researchers around the world have developed ocean energy devices over the last three decades, such as fixed and floating offshore wind turbines and wave and tidal energy converters. Furthermore, experimental facilities designed to test such devices have become increasingly focused on the generation of multidirectional, realistic, waves. In particular, FloWave, located at the University of Edinburgh in Scotland, is the first ocean energy research facility in the world to reproduce wave and current combinations to realise sea states that include severe design conditions in a multidirectional circular water tank.

In this study, a numerical water tank model was developed for the FloWave multidirectional wave basin using a modified version of DualSPHysics on graphics processing units. The geometry includes 168 wave-maker paddles that were constructed using particles and treated as a solid phase. Rotation angle data was individually imposed on each paddle to generate monochromatic long-crested regular/irregular wave trains and a concentric wave singularity including wave absorption. Model-determined surface elevation results were in overall agreement with the experimental results; Several regular, irregular and concentric wave conditions were successfully reproduced in a multidirectional wave basin. The presented research represents the first reported reproduction of a multi-directional wave tank, and multi-directional waves, using particle based methods. To demonstrate future capability, the numerical model was also applied to a strong fluid-structure interaction between wave trains and an offshore wind turbine structure with six degrees of freedom as a further work.

A study is on-going to include flow generators with impellers to generate tidal currents and combinations of waves and currents as real sea state conditions. The spatial distributions of the flow field from the numerical model will be validated with coastal acoustic tomography (CAT) performed in the FloWave.

KEYWORDS
SPH; particle based method; multidirectional circular wave basin; FloWave; ocean energy

CONTACT Mutsuda, H. Email: mutsuda@hiroshima-u.ac.jp

1. Introduction

In recent years, there has been significant interest in the generation of offshore renewable energy. Research groups around the world over the last three decades have been developing various ocean energy devices, such as a fixed and floating offshore wind turbines and wave and tidal energy converters.

Experimental reproductions of realistic directional sea states have been performed at a variety of multidirectional wave tanks, including the circular AMOEBA tank (Minoura et al. (2009)) with an element-absorbing wave maker at Osaka University, the 15-m deep sea basin with 128 absorbing wave makers at the National Maritime Research Institute of Tokyo in Japan and the 2013 FloWave Ocean Energy Research Facility at the University of Edinburgh in Scotland (FloWave (2018)), as shown in Fig.1. FloWave is the first basin in the world to enable the generation of waves and currents at arbitrary angles, enabling the creation of severe multidirectional design conditions (Ingram et al. (2014)). The FloWave has 168 absorbing wave-maker hinged-type paddles to generate both traditional monochromatic waves and full-spectrum multidirectional waves. International research has been carried out in the FloWave basin (Draycott et al. (2015), Draycott et al. (2016), Draycott et al. (2018), Sutherland et al. (2017a), Sutherland et al. (2017b), Ordonez-Sanchez et al. (2017)), designing ocean energy converters and investigating the performance and loads in specific sea conditions before installing them in real test locations, such as the Orkney Islands in UK or Nagasaki in Japan. However, a powerful computational tool to utilise experimental results and conduct design-based simulations has not yet been developed for FloWave. Particle-based methods without grids and re-meshing techniques are more suitable for constructing a multidirectional water tank and for computing strong fluid-structure interactions between ocean energy facilities and breaking waves compared with ordinary grid-based methods such as VOF method (Hirt et al. (1981)), Level-set method (Osher et al. (1988)) and CIP method (Yabe et al. (2001)).

A recent review based on particle-based methods can be found in Gotoh et al. (2018) for coastal and ocean engineering. In particular, wave generation and propagation are a critical issue in any numerical and physical model employed in coastal and ocean engineering purposes. In recent works for developing numerical tanks using meshless models, Altomare et al. (2017) investigated wave generation and active wave absorption for second-order long-crested monochromatic and random waves by

Figure 1. FloWave, an ocean energy research facility (FloWave (2018), Ingram et al. (2014)), constructed at the University of Edinburgh in Scotland, see in *https* : *//www.flowavett.co.uk/home*.

a WCSPH-based (Weakly Compressible Smoothed Particle Hydrodynamics) model. Wen et al. (2018) also demonstrated generation and propagation of regular and random waves using a parallel SPH model. Moreover, Farhadi et al. (2016) investigated and compared the accuracy of solitary wave generation techniques by several mesh free schemes based on a ISPH (Incompressible Smoothed Particle Hydrodynamics) model. Khayyer et al. (2018) developed a projection-based SPH method for a numerical wave flume with porous media and Gunn et al. (2018) demonstrated wave an interaction problem with a tethered buoy using SPH. Some papers regarding wave-structure interaction problems (Le et al. (2010), Gomez et al. (2012), Gotoh et al. (2016), Hwang et al. (2016) and Zhang et al. (2017)) have been also investigated in recent years. However, most of these works have been widely applied to a 2D numerical wave tank, not a multidirectional wave basin with individually controlled wave paddles in 3D using particle based methods. Therefore, to the best knowledge of authors, no research works construct and validate a multi-directional wave basin with multi-directional waves in 3D.

Here, a numerical water tank for the multidirectional wave basin FloWave was developed using a particle-based method, DualSPHysics (Crespo et al. (2015)), based on smoothed particle hydrodynamics (SPH) (Gingold et al. (1977)). Wave elevation and propagation were validated using experimental results of long-crested regular/irregular waves and a concentric wave singularity in a multidirectional wave basin. The presented research represents the first reported reproduction of a multi-directional wave tank, and multi-directional waves, using particle based methods. The model was subsequently used to demonstrate fluid-structure interaction between waves and an offshore wind turbine as a further work.

2. Numerical method

To compute a strongly nonlinear free-surface flow in a large focused domain, such as FloWave with a diameter and a water depth of 25 m and 2 m, respectively, a high performance and powerful computer should be used with a powerful central processing unit (CPUs) and graphic processing unit (GPUs). GPU computing is an affordable option to compute large computational domains because GPUs are designed to manage large amounts of data whilst offering higher computing power than CPUs. Thus, the SPH-based (Gingold et al. (1977)), open-source, parallel computational fluid dynamics solver DualSPHysics (Crespo et al. (2015)) was used. Modifications were made to the code to generate regular and irregular wave trains to reproduce several sea state conditions created by a hinged-type wave maker and to compute strongly nonlinear free-surface flow and fluid-structure interaction problems in FloWave.

2.1. *SPH*

SPH is a particle-based method developed by Gingold et al. (1977) to track fluid motion as a set of discrete elements, called particles. Physical quantities defined on each particle can be computed by a spatial interpolation of neighbouring particles having a smoothing length, a circle in 2D and a sphere in 3D. At each time step, a new physical quantity on each particle can be evaluated and time integration for acceleration, velocity and location for each particle can be updated by using the SPH discretisation.

The fundamental principle of the SPH method, as shown in Fig.2, is to approximate

the physical quantity ϕ :

$$\phi(\mathbf{r}) = \int_{\Omega} \phi(\mathbf{r}')W(\mathbf{r} - \mathbf{r}', h)d\mathbf{r}' \tag{1}$$

where W is the kernel function, h is the referenced length, $\mathbf{r}$ is the focused position vector, Ω is the referenced area with a radius to evaluate interaction between particles and $\mathbf{r}'$ is the neighbouring position vector. This equation can be expressed in a discrete form as below:

$$\phi(\mathbf{r}_i) \approx \sum_j \phi(\mathbf{r}_j)W(\mathbf{r}_i - \mathbf{r}_j, h)V_j \tag{2}$$

where i is a focused positon particle and V_j is the volume of a neighbouring particle j. The relation shown in Eq.(2) should be also satisfied:

$$\sum_j W(\mathbf{r}_i - \mathbf{r}_j, h) \approx 1 \tag{3}$$

If $V_j = m_j/\rho_j$, where m and ρ represent the mass and density of particle j, respectively, then Eq.(3) can be reformulated:

$$\phi(\mathbf{r}_i) \approx \sum_j \phi(\mathbf{r}_j)\frac{m_j}{\rho_j}W(\mathbf{r}_i - \mathbf{r}_j, h) \tag{4}$$

where the kernel function W is a Quintic Kernel, as follows:

$$W(\mathbf{r}_i, h) = \alpha_D \left(1 - \frac{q}{2}\right)^4 (2q + 1), \quad 0 \leq q \leq 2 \tag{5}$$

where α_D is equal to $21/16\pi h^3$ in 3D. Eq.(4) and its derivative in space can be applied to the governing equations in fluid phase.

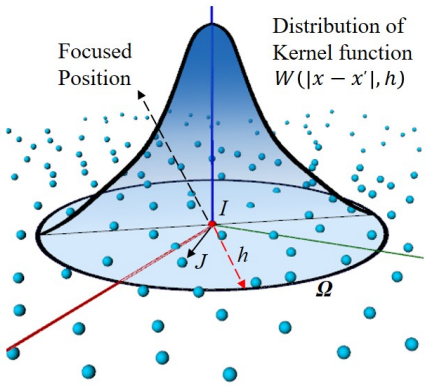

Figure 2. The fundamental principle of the SPH method represented by distribution of a Kernel function with a referenced distance, h.

2.2. *Governing equations and time integration*

Using Eq.(4) and its derivative with an artificial viscosity scheme proposed by Gingold et al. (1977) in the SPH manner and assuming a continuum, the momentum equation can be written as

$$\frac{d\mathbf{v}_a}{dt} = -\sum_j m_j \left(\frac{P_j}{\rho_j^2} + \frac{P_i}{\rho_i^2} + \Pi_{ij} \right) \nabla_i W_{ij} + \mathbf{g} \tag{6}$$

where $\mathbf{v}_a$ is the velocity in 3D, $P_{i,j}$ and $\rho_{i,j}$ are the pressure and the density, respectively, corresponding to particles i and j, $\mathbf{g}$ is the gravitational acceleration and Π_{ij} is the viscosity term given by

$$\Pi_{ij} = \begin{cases} \frac{-\alpha \bar{c}_{ij} \mu_{ij}}{\bar{\rho}_{ij}} & \mathbf{v}_{ij} \cdot \mathbf{r}_{ij} \leq 0 \\ 0 & \mathbf{v}_{ij} \cdot \mathbf{r}_{ij} > 0 \end{cases} \tag{7}$$

where $\mathbf{r}_{ij} = \mathbf{r}_i - \mathbf{r}_j$ and $\mathbf{v}_{ij} = \mathbf{v}_i - \mathbf{v}_j$ are the particle position and velocity respectively, $\mu_{ij} = h\mathbf{v}_{ij} \cdot \mathbf{r}_{ij} / (r_{ij}^2 + \eta^2)$ with $\eta^2 = 0.01h^2$, $\bar{c}_{ij} = 0.5(c_i + c_j)$ is the mean speed of sound c and α is a tuning parameter coefficient for proper dissipation. The recommended value of $\alpha = 0.01$ to investigate wave propagation and wave loadings exerted onto coastal and ocean structures was assumed here (Crespo et al. (2015)).

Fluid is treated as weakly compressible; an equation of state is employed to compute pressure based on particle density. Assuming a weakly compressible fluid using the SPH formulation, the mass of each particle remains constant, including their associated fluctuations. The density changes can be computed by solving the continuity equation using the SPH manner:

$$\frac{d\rho_i}{dt} = -\sum_j m_j \mathbf{v}_{ij} \cdot \nabla_i W_{ij} \tag{8}$$

where ρ_i is the density at the particle position i. The pressure in the fluid, P, is based on the equation of state that can be expressed as follows:

$$P = b \left[\left(\frac{\rho}{\rho_0} \right)^{\gamma} - 1 \right] \tag{9}$$

where $\gamma = 7$, $b = c_0^2 \rho_0 / \gamma$, $\rho_0 = 1000\ \mathrm{kg/m^3}$ is the referenced density and c_0 is the sound speed represented by $c_0 = \sqrt{\partial P / \partial \rho}$. There is no need to solve Poisson's equation for the pressure used in the computational algorithm, Simplified marker and cell (SMAC) method for an incompressible fluid.

The numerical scheme used is an explicit second-order Symplectic integration algorithm with accuracy in time of $O(\Delta t^2)$ and involves predictor and corrector stages as

below:

$$\mathbf{r}_i^{n+1/2} = \mathbf{r}_i^n + \frac{\Delta t}{2}\mathbf{v}_i^n \tag{10}$$

$$\rho_i^{n+1/2} = \rho_i^n + \frac{\Delta t}{2}D_i^n \tag{11}$$

$$\mathbf{v}_i^{n+1} = \mathbf{v}_i^{n+1/2} + \frac{\Delta t}{2}\mathbf{F}_i^{n+1/2} \tag{12}$$

$$\mathbf{r}_i^{n+1} = \mathbf{r}_i^{n+1/2} + \frac{\Delta t}{2}\mathbf{v}_i^{n+1} \tag{13}$$

where $\mathbf{F}$ consists of pressure gradient term, diffusion term and gravitational acceleration term, the subscript n indicates the time step and Δt is the time increment for n-step. The corrected density, $d\rho_i^{n+1}/dt = D_i^{n+1}$, where D is the divergence, can be computed using $\mathbf{v}_i^{n+1}$ and $\mathbf{r}_i^{n+1}$ at the next time step, n+1.

In this study, the viscosity treatment was based on the artificial viscosity using Eq.(7) and Delta-SPH (Antuono et al. (2010), Marrone et al. (2011)) was also used for a diffusive term to reduce density fluctuations. The shifting algorithm (Xu et al. (2009)) for particle spacing was not employed in this study. A quintic function (Wendland (1995)) was selected as a smoothing kernel.

2.3. *Motions of floating body in 6 DOF*

To compute the motion of a moving body, such as a floating structure or a ship, with six degrees of freedom (6 DOF), rigid body dynamics (Baraff (1997)) can be used. The basic equations can be written as follows:

$$M\frac{d\mathbf{V}_b}{dt} = \sum_k m_k\mathbf{f}_k \tag{14}$$

$$I\frac{d\mathbf{\Omega}_b}{dt} = \sum_k m_k(\mathbf{r}_k - \mathbf{R}_0)\times\mathbf{f}_k \tag{15}$$

where M is the mass of the body, I is the inertia moment, $\mathbf{v}_b$ is the velocity of the rigid body, $\mathbf{\Omega}_b$ is the rotational velocity of the body, $\mathbf{f}$ is the net force consisting of gravitational force and the exciting force acting on each particle at the solid boundary. The net force on each boundary particle can be calculated by all surrounding fluid particles referred by the kernel function and the smoothing length, $\mathbf{R}_0$ is the centre of gravity and k indicates the boundary particle on the rigid body surface. Thus, force contributions for the entire rigid body are summed. After calculating the velocity and the rotational velocity of the rigid body using Eq.(14) and Eq.(15), the velocity of each particle $\mathbf{v}_i$ on the rigid body surface can be represented by

$$\mathbf{v}_i = \mathbf{V}_b + \mathbf{\Omega}_b \times (\mathbf{r}_i - \mathbf{R}_0). \tag{16}$$

The numerical code based on DualSPHysics (Crespo et al. (2015)) was optimised using good practice approaches for CPU-GPU computations in SPH code with accuracy, reliability and robustness given during computational time. Both C++ and CUDA of the code contained the same features and options. Most of the source code was common to CPU and GPU in this study.

3. Application to the FloWave Ocean Energy Research Facility

3.1. *Motion of a hinged-flap wave maker in the FloWave*

The FloWave basin is the world's first circular combined wave-current facility. The basin was designed to test a multitude of offshore structures and ocean energy devices such as tidal current turbines, wave energy devices and fixed or floating offshore wind turbines. The FloWave has a circular 25 m diameter test area with 2 m of water depth. Combinations of waves and currents are generated using 28 independently controlled 1.7-m diameter impellers and 168 hinged-flap type wave makers with force-feedback control. The 168 active-absorbing paddles can create both traditional monochromatic and full-spectrum multidirectional waves and can be controlled by the far-field Biesel transfer function (Frigaard et al. (2010)) between wave amplitude and paddle displacement:

$$S(z) = \begin{cases} S_0 \cdot \frac{h+z-h_0}{h-h_0} & (z+h) \geq h_0 \\ 0 & (z+h) < h_0 \end{cases} \tag{17}$$

$$\frac{H}{S_0} = \frac{2}{k(h-h_0)} \times \left[\frac{\sinh(kh)\left\{k(h-h_0)\sinh(kh) - \cosh(kh) + \cosh(kh_0\right\}}{\sinh(kh)\cosh(kh) + kh} \right] \tag{18}$$

where $S(z)$ depending on the rotation angle ω at the hinge is the stroke of the paddle at the vertical position z; $S(0) = 0$ when $z = 0$. H is the far-field wave height and h is the water depth.

The far-field Biesel transfer function used for evaluating a hinged-type wave maker is shown in Fig.3. Each absorbing wave-maker paddle was represented by SPH particles and treated as a solid model governed by Eq.(14) and Eq.(15). The flap motion of the wave paddles was imposed as a boundary condition along the circumference of the FloWave tank by using Eq.(17) regarding the stroke $S(z)$ and the rotation angle ω. Wave generation validation was conducted using long-crested regular and irregular waves, along with a concentric wave singularity resulting in a highly non-linear breaking wave. The rotation angle and stroke of each paddle was individually controlled by a signal based on the far-field Biesel transfer function.

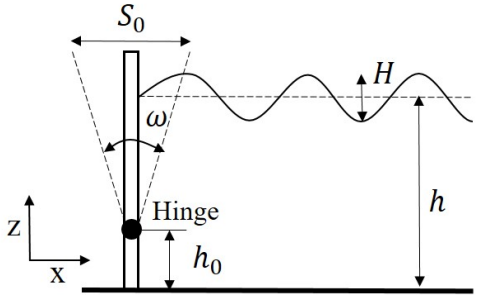

Figure 3. Far-field Biesel transfer function for an elevated hinged-type wave maker.

To reproduce the aforementioned wave conditions, first the paddle angles for each of

the 168 wavemakers have been recorded at FloWave for each of the modelled sea states. These recorded paddle angles are then imposed in the SPH model. This approach ensures that exactly the same boundary conditions have been applied between model and experiment; enabling differences to be directly attributed to the model implementation. In addition, this approach ensures that the complex real-time force-feedback wavemaker control is implicitly included in the model and reflections are realistic. The nature and level of reflections in the FloWave tank can be found in Draycott et al. (2016).

An example of a rotation angle from the elevated hinged-type wave maker generating water waves at each condition and arrangement is shown in Fig.4 from the top view of the paddles located at the circuit clockwise in FloWave. When generating a regular wave by the 168 wave-maker paddles, both paddle phases and amplitudes are controlled to ensure accurate generation and absorption. Similarly, for irregular wave generation the phases and amplitudes of paddles are controlled considering the desired wave amplitude and phases for the frequency components of the sea state. To generate the concentric singularity (spike wave), phases are manipulated to ensure all frequency–direction components are in phase at the desired focus time and position. This circular focused wave is rotationally symmetric, and as such results in all paddles undergoing the same motion (see Fig.4). Wave gauge positions and the coordinate system are shown in Fig.5. Surface elevations were measured by eight multiplexed resistance-type wave gauges with a sampling frequency of 32 Hz near the centre of the FloWave basin to pick up and focus on the time series of surface waves. Time-series of surface elevations measured at these locations are compared with model results, as shown in the next sections. The designed waves could be produced and absorbed in every direction: $\theta = 0$ deg. for regular waves, $\theta = 90$ deg. for irregular waves and multi-direction for concentric spike waves.

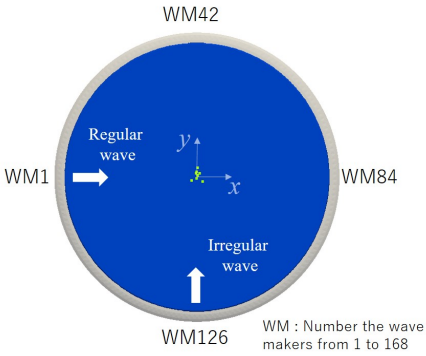

(a) Arrangement of the 168 wave paddles in FloWave.

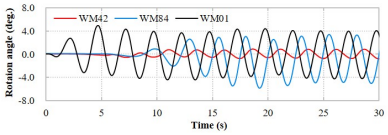

(b) Regular wave.

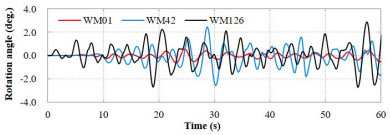

(c) Irregular wave.

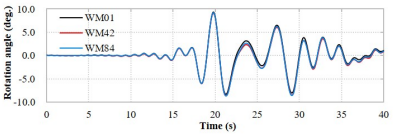

(d) Concentric wave.

Figure 4. Rotation angle of elevated hinged-type wave makers to generate water waves.

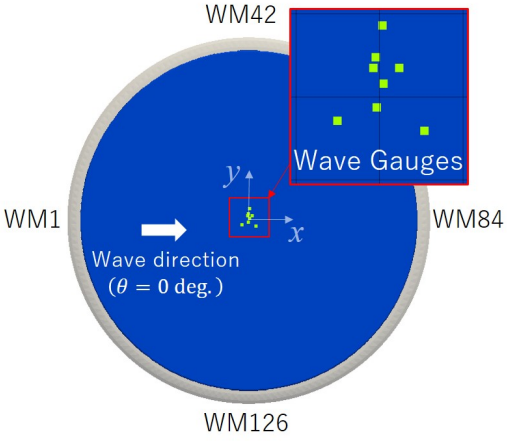

(a) Regular wave.

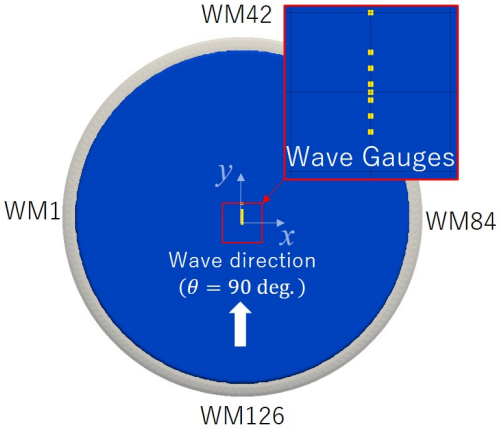

(b) Irregular wave.

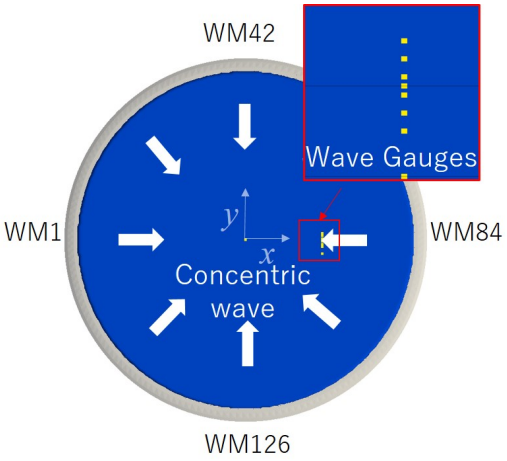

(c) Concentric wave as a spike wave.

Figure 5. Positions of wave gauges measuring water elevation.

Table 1 shows the wave conditions used in this study. Regular and irregular wave conditions in long-crested wave trains were first demonstrated and validated by water surface elevation with experimental data in FloWave. For the regular wave conditions, the frequency ranges were set from 0.4 to 0.6 Hz with a wave height H from 0.087 to 0.195 m, wave period T from 1.67 to 2.5 s with a steepness (defined as H/L) of 0.02. The simulation time was 30 s, in which around 7 to 11 wave trains, depending on the wave period, were propagated and reproduced in FloWave. Two Pierson Moskowitz spectra (H_{m0}=0.075 $\sim$ 0.15 m, T_p=1.5 $\sim$ 3.0 s) with a uniform propagation direction of 90 deg. was next performed in the FloWave to generate long-crested irregular wave trains. The random wave trains were generated by an inverse Fourier transform method with randomised component phases and were strictly deterministic. Finally, a concentric wave singularity was demonstrated, creating a focused spike wave which can be viewed as 'inverse stone throwing problem'. The simulation time was 60 s.

The initial distance d_p/D between SPH particles in the computational model was set to 4.0×10^{-3}, 2.0×10^{-3} and 1.1×10^{-3}, where D is the diameter of the FloWave, to validate convergence. The total number of SPH particles including wave paddles and tank bottom was about 1.2 million for the coarse particle and 52 million particles for fine particle. The total number may be considered a coarse condition for wave propagation, but these conditions were a preliminary validation and the first demonstration for the FloWave was numerically performed using GPU and CPU. The runtime was less than one hour for coarse particles, and about one hundred hours for finer particles by using only one GPU (GeForce GTX 1080Ti) without a parallel computing.

The comparison of water elevation should be quantitatively investigated and the convergence rate should be carefully examined. In this study, RMSE (Root mean square error) in time variation of water elevation between experimental and numerical results is shown in Table 1. It can be seen that the numerical results in finer particle cases were gradually converged and the accuracy is relatively higher in regular, irregular and spike waves.

Table 1. Incident wave conditions.

Condition	H*3 (m)	T*4 (s)	H/L	d_p/D*5	RMSE*6
Regular	0.195	2.5	0.02	4.0×10^{-3}	0.0108
Regular	0.195	2.5	0.02	2.0×10^{-3}	0.0104
Regular	0.087	1.67	0.02	4.0×10^{-3}	0.0155
Regular	0.087	1.67	0.02	1.1×10^{-3}	0.0065
Irregular	0.150	1.5		4.0×10^{-3}	0.0314
Irregular	0.150	1.5		2.0×10^{-3}	0.0218
Irregular	0.150	1.5		1.1×10^{-3}	0.0189
Irregular	0.075	3.0		4.0×10^{-3}	0.0130
Irregular	0.075	3.0		2.0×10^{-3}	0.0089
Irregular	0.075	3.0		1.1×10^{-3}	0.0076
Spike*1				4.0×10^{-3}	0.0355
Spike				2.0×10^{-3}	0.0181
Spike				1.1×10^{-3}	0.0172
FSI*2 in Regular	0.195	2.5	0.02	1.1×10^{-3}	
FSI in Spike				1.1×10^{-3}	

*1 Spike : Concentric wave singularity, *2 FSI : Fluid Structure Interaction, *3 H : Wave height in regular waves and significant wave height in irregular waves, *4 T : Wave period in regular waves and peak wave period in irregular waves, *5 D : Diameter of FloWave, d_p: particle size, *6 RMSE : Root mean square error

3.2. *Regular waves*

A snapshot of water surface elevation and wave propagation in the wave tank model is shown in Fig.6. Long-crested regular wave trains from left to right on the x-axis were repeatedly produced and absorbed downstream by controlling the 168 wave paddles without disturbance. Model and experimental water surface elevation times series at the centre of wave gauge 1 (WG1 as shown in Fig.5) are compared in Fig.7. The fine particle models ($d_p/D = 1.1 \times 10^{-3}$ and $d_p/D = 2.0 \times 10^{-3}$) were in good agreement with the experimental results, especially in the wave amplitude. Convergence was also verified in this model. However, the water surface elevation time histories have a small discrepancy among them and their phase was slightly and gradually shifted because numerical instability might be occurred during long-time integration. The set-up phenomena due to wave drift was generated at the end; the model should be modified in the future to consider this.

Figure 6. Snapshot of wave propagation in regular wave conditions (wave direction : from left to right).

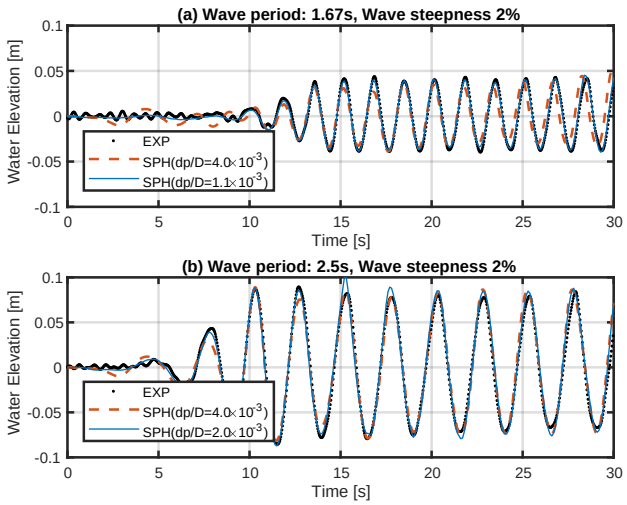

Figure 7. Water elevation time variation in regular wave conditions.

3.3. *Irregular waves*

A snapshot of long-crested irregular wave propagation from a wave direction of 90 deg. in y-axis is presented in Fig.8. The designed irregular wave trains were generated by the Pierson Moskowitz spectrum without disturbance by the 168 hinged-flap type wave makers. Water surface elevations time variation for the wave conditions, T_p=1.5 s, H_{m0}=0.15 m and T_p=3.0 s, H_{m0}=0.075 m with $d_p/D = 1.1 \times 10^{-3}$ are shown in Fig.9; experimental results were measured by WG1 in Fig.5. The computational results were in good agreement with the experimental results, especially in the time 10 s $\leq t \leq$ 50 s. However, there were large discrepancies in the amplitude and phase when $t >$ 50 s. This could have been caused by the reflected wave with numerical instability from the downstream side of the wave paddle, even though the wave makers were individually controlled, actively absorbing and contained force feedback. In future study, the active control should be strictly followed and the numerical disturbance should be decreased by some improvements.

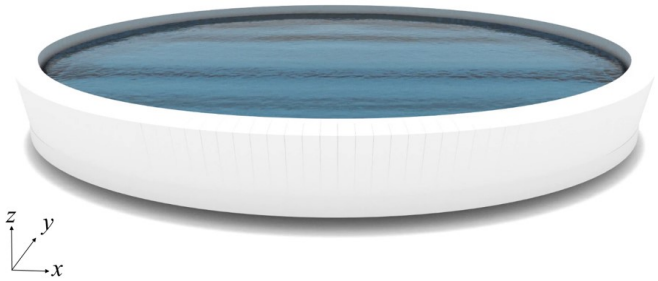

Figure 8. Snapshot of wave propagation in irregular wave conditions (wave direction : from front to back).

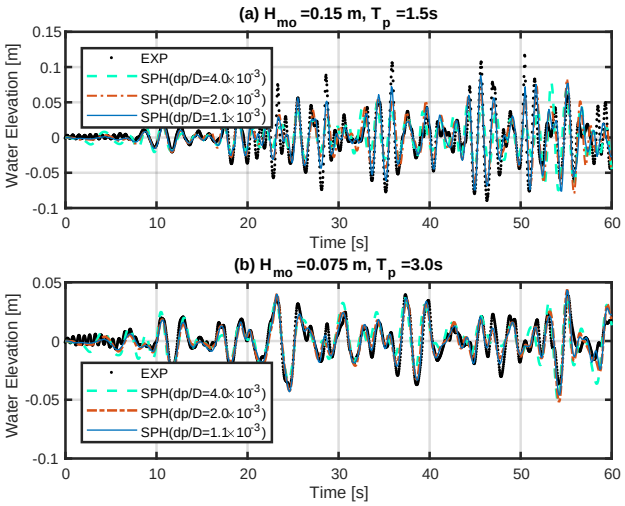

Figure 9. Water elevation time variation in irregular wave conditions.

3.4. *Concentric wave singularity –Spike wave*

The numerical model was applied to generate a concentric wave singularity as a spike wave, demonstrated as the 'inverse stone throwing problem'. A signal for each of the 168 wave paddles was imposed to produce a circular wave which breaks at the centre of the FloWave. The concentric wave singularity causes highly nonlinear surface motion with breaking, splashing and jet ejection.

A snapshot of the concentric wave singularity with jet ejection and wave breaking under the varying spatial resolution ($d_p/D = 4.0 \times 10^{-3}$, $d_p/D = 2.0 \times 10^{-3}$ and $d_p/D = 1.1 \times 10^{-3}$) is shown in Fig.10. Water elevation of the strongly nonlinear spike wave, measured via wave gauge 4 at the centre point of the FloWave, ($x = 0$, $y = 0$), is shown in Fig.11. The maximum isolated wave height reached over 4 m, also known as a freak or pyramidal wave. The maximum water surface was reproduced and sharpened when employing fine particles ($d_p/D = 1.1 \times 10^{-3}$). Computational and experimental wave patterns were similar, but the computational model underestimated the maximum wave height and did not accurately reproduce the free high-frequency wave. This is because the particle size was relatively large for the tracking of nonlinear surface motion with violent breaking. The full crest amplitude of the spike wave is known to be in excess of 5 m, and as such finer particles are expected to be required to accurately model this phenomenon. More detailed validation with smaller-sized particles should be computed in future study.

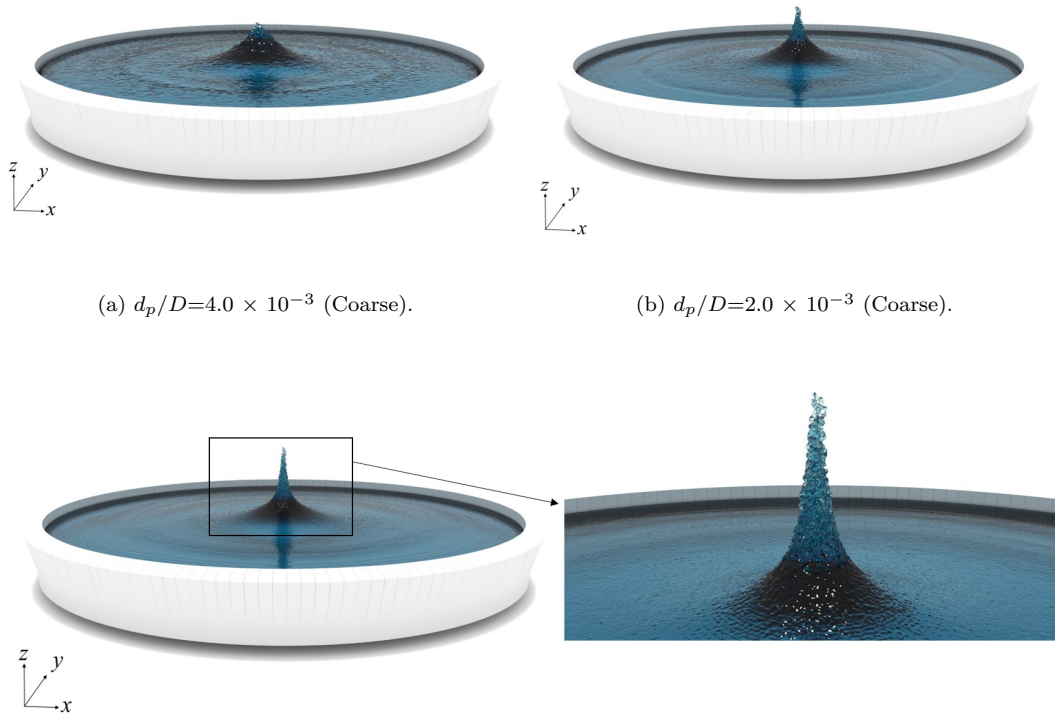

(a) d_p/D=4.0 × 10^{-3} (Coarse).

(b) d_p/D=2.0 × 10^{-3} (Coarse).

(c) d_p/D=1.1 × 10^{-3} (Fine).

Figure 10. Snapshot of water elevation in a concentric wave singularity.

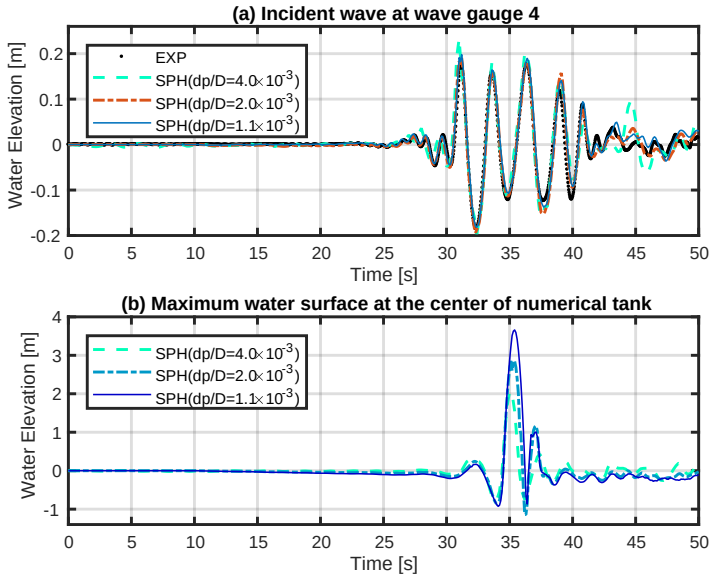

Figure 11. Water elevation time variation in a concentric wave singularity.

4. Further work

The previous sections showed the validation and accuracy in wave generation, propagation and reflection in the numerical multidirectional circular wave basin using SPH. In this section, we demonstrate the future capability of the numerical wave basin presenting preliminary results of fluid-structure interaction. Validation of this capability is an area for extensive future work.

One example of interaction between a regular wave (wave amplitude: 0.195 m, wave period: 2.5 s, wave steepness: 2%) and a floating offshore wind turbine with drift motion without mooring, is presented in Fig.12. The particle size was $d_p/D = 1.1 \times 10^{-3}$ and the total number of particles was about 47 million. The floating motion of the offshore wind turbine was computed with 6 DOF. The displacement and rotation angle with time are presented in Fig.13. The heave and pitch motions were repeatedly excited by the regular wave train and the surge motion in x-axis was generated by the drift force; however, the sway and yaw motions were quite small.

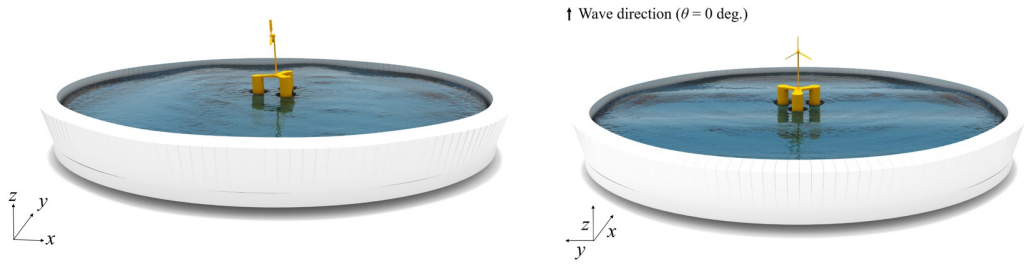

(a) Side view. (b) Front view.

Figure 12. Fluid-structure interaction between a regular wave and a floating offshore wind turbine.

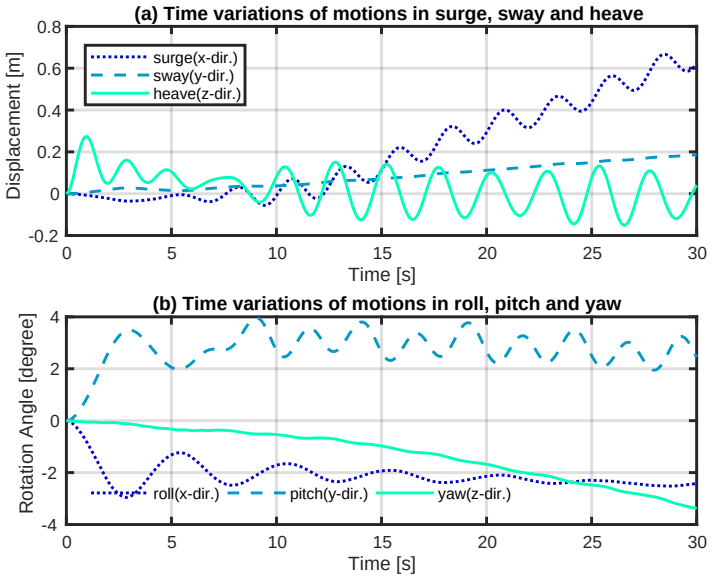

Figure 13. 6-DOF motions of the floating offshore wind turbine in the regular wave.

Next example of fluid-structure interaction between a concentric wave singularity and an offshore wind turbine with 6 DOF, as demonstrated in Fig.10, is presented in Fig.14. Here the particle size was also set to $d_p/D = 1.1 \times 10^{-3}$ with a total number of particles of about 47 million. The strong splashing on the bottom surface of the floater lifted it from the free surface. The time histories of motions in 6 DOF are shown in Fig.15. The dominant heave motion occurred at the centre of FloWave, which is very large, over 1 m in z-direction and the floater freely oscillated with natural frequency. All floater motion should be validated with experimental data; future study will include fluid-structure interactions with ocean energy convertors in real sea state conditions.

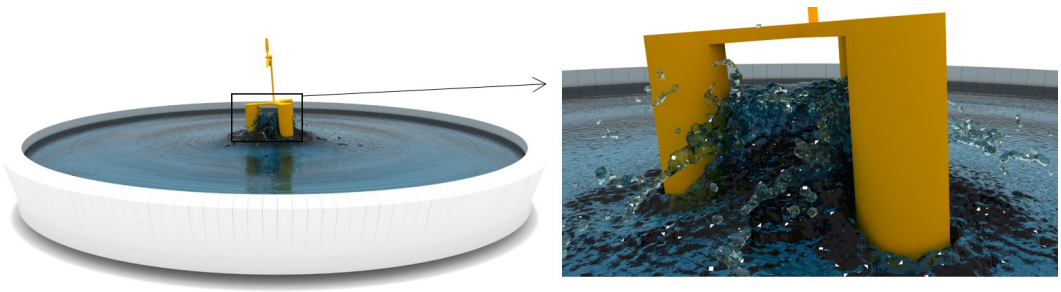

Figure 14. Fluid-structure interaction between a concentric wave and a floating offshore wind turbine; left : whole area, right: enlarged area near the bottom surface of the floating body.

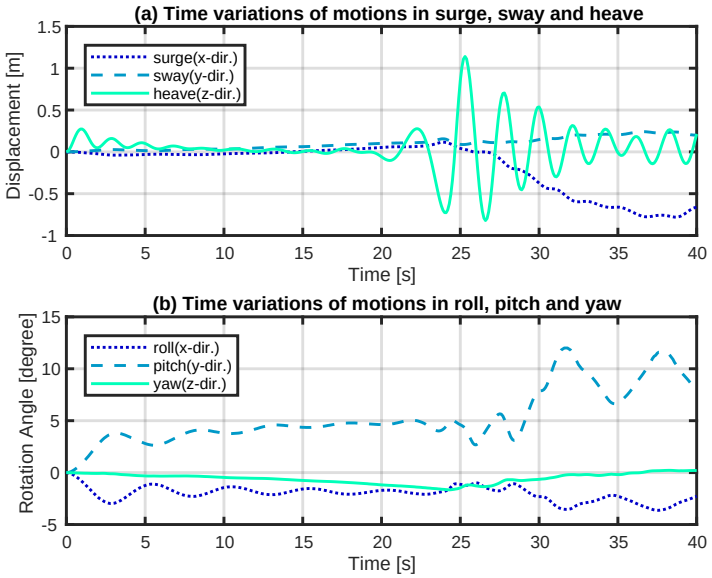

Figure 15. 6-DOF motions of the floating offshore wind turbine in the concentric wave.

5. Conclusions

A numerical water tank model for the FloWave multidirectional circular wave basin was developed using DualSPHysics based on Smoothed Particle Hydrodynamics. The model contained 168 hinged-flap type wave makers and reproduced long-crested regular and irregular waves and a concentric wave singularity in a multidirectional wave basin. This represented the first documented research to use particle methods simulate and validate multi-directional waves in a multi-directional wave tank. Model surface elevation time variation results were in good agreement with experimental results. The numerical model was also applied to fluid-structure interaction problems between waves and a floating offshore wind turbine. More detailed validations will be done as future study.

Further effort is on-going to generate short-crested waves with several spreading parameters and also to include a flow generator with impellers to reproduce tidal currents and combination of waves and currents in real sea state conditions. Model spatial distributions of current fields in the FloWave will be validated with the CAT system (Taniguchi et al. (2010)) conducted by Li et al. (2017) in the University of Edinburgh and Prof. Kaneko in Hiroshima University.

Acknowledgements

This study was supported in part by Grants-in-Aid for Scientific Research (B), KAKENHI (17H03494) , Fundamental Research Developing Association for Shipbuilding and Offshore (REDAS) and The Hiroshima University Education and Research Support Foundation. The experimental data from the FloWave was provided by the collaborators in the Institute for Energy Systems of the University of Edinburgh, Scotland. The authors express thanks for all of the support.

References

Altomare, C., Domnguez, J. M., Crespo, A. J. C., Gonzalez-Cao, J., Suzuki, T., Gomez-Gesteira, M., Troch, P. 2017. "Long-crested wave generation and absorption for SPH-based DualSPHysics model." *Coastal Engineering.* 127: 37-54.

Antuono, M., Colagrossi, A., Marrone, S., Molteni, D. 2010. "Free-surface flows solved by means of SPH schemes with numerical diffusive terms." *Comput. Phys. Commun.* 181: 532-549.

Baraff, D. 1997. "An Introduction to Physically Based Modeling: Rigid Body Simulation I, Unconstrained Rigid Body Dynamics, – Rigid Body Simulation –." *SIGGRAPH 97 course notes.* 1-31.

Crespo, A. J. C., Dominguez, J. M., Rogers, B. D., Gomez-Gesteir, M., Longshaw, S., Canelas, R., Vacondio, R., Barreiro, A., Garcia-Feal, O. 2015. "DualSPHysics: open-source parallel CFD solver on Smoothed Particle Hydrodynamics (SPH)." *Computer Physics Communications.* 187: 204-216.

Draycott, S., Davey, T., Ingram, D., Lawrence, L., Day, A., Johanning, L. 2015. "Using a Phase-Time-Path-Difference Approach to Measure Directional Wave Spectra in FloWave." *Proceeding of European Wave and Tidal Energy Conference.* EWTEC.

Draycott, S., Davey, T., Ingram, D, Day, A., Johanning, L. 2016. "The SPAIR method : Isolating incident and reflected directional wave spectra in multidirectional wave basins." *Coastal Engineering.* 114: 265-283.

Draycott, S., Steynor, J., Davey, T., Ingram, D. 2018. "Isolating incident and reflected wave spectra in the presence of current." *Coastal Engineering Journal.* 60: https://doi.org/10.1080/05785634.2017.1418798.

Farhadi, A., Ershadi, H., Emdad, H., Rad, E. G. (2016). "Comparative study on the accuracy of solitary wave generations in an ISPH-based numerical wave flume." *Allied Ocean Research.* 54: 115-136.

FloWave, https://www.flowavett.co.uk/home (accessed August 2018).

Frigaard, P., Brorsen, M. 1995. "A Time-Domain Method for Separating Incident and Reflected Irregular Waves." *Coastal Engineering.* 24 (34): 205215

Gingold, R. A., Monaghan, J. J. 1977. "Smoothed particle hydrodynamics: theory and application to non-spherical stars." *Mon. Not. R. Astron. Soc.* 181: 375389.

Gomez-Gesteria, M., Rogers, B. D., Crespo, A. J. C., Dalrymple, R. A., Narayanaswamy, M., Dominguez, J. M. 2012. "SPHysics-development of a free-surface fluid solver - Part 1 : Theory and formulations." *Computers & Geosciences.* 48: 289-299.

Gotoh, H., Khayyer, A. 2016. "Current achievements and future perspectives for projection-based particle methods with applications in ocean engineering." *Journla of Ocean Eng. and Mar. Eng.* 2(3): 251-278.

Gotoh, H., Khayyer, A. 2018. "On the state-of-the-art of particle methods for coastal and ocean engineering." *Coastal Engineering Journal.* 60: 79-103.

Gunn, D. F., Rudman, M., Cohen, R. C. Z. 2018. "Wave interaction with a tethered buoy: SPH simulation and experimental validation." *Ocean Engineering.* 156: 306-317.

Hirt, C. W., Nichols, B. D. 1981. "Volume of Fluid (VOF) method for the dynamics of free boundaries." *Journal of Computational Physics.* 39: 201-225.

Hwang, SC., Park, J. C., Gotoh, H., Khayyer, A. Kang, K. J. 2016. "Numerical simulations of sloshing flows with elastic baffles by using a particle-based fluid-structure interaction analysis method." *Ocean Engineering.* 118: 227-241.

Ingram, D., Wallace, R., Robinson, A. and Bryden, I. 2014. "The design and commissioning of the first, circular, combined current and wave test basin." *Proceedings of Oceans 2014 MTS/IEEE.* IEEE. 131217-002.

Khayyer, A., Gotoh, H., Shimizu, Y., Gotoh, K., Falahaty, H., Shao, S. 2018. "Development of a projection-based SPH method for numerical wave flume with porous media of variable porosity." *Coastal Engineering.* 140: 1-22.

Le, T. D., Marsh, A., Oger, G., Guilcher, P. M., Khaddaj-Mallat, C., Alessandrini, B., Ferrant,

P. 2010. "SPH simulation of gree water and ship flooding scenarios." *Journla of Hydrodynamics.* Ser. B 22 (5) : 231-236

Li, G., Ingram, D., Kaneko, A., Gohda, N., Noble, N., Mutsuda, H., Polydorides, N. 2017. "Flow generation and testing in a circular experimental basin." *Proceedings of Offshore Energy and Storage.*

Marrone, S., Antuono, M., Colagrossi, A., Colicchio, G., Le, Touze, D., Graziani, G. 2011. "Delta-SPH model for simulating violent impact flows." *Comput. Meth. Appl. Mech. Eng.* 200: 1526-1542.

Minoura, M., Takahashi, R., Okuyama, E., Naito, S. 2009. "Generation of extreme wave composed of ring waves in a circular basin." *Proceedings of the 19th International Offshore and Polar Engineering Conference.* 389-396.

Ordonez-Sanchez, S., Duncan, S., Grgory, P., Tom, B., Mulualem, G., Michael, B., Ian, M. 2017. "Experimental evaluation of the wake characteristics of cross flow turbine arrays." *Ocean Engineering.* 141: 215-226. 10.1016/j.oceaneng.2017.06.035.

Osher, S. and Sethian, J. A. 1988. "Fronts Propagating with Curvature Dependent Speed: Algorithms Based on Hamilton-Jacobi Formulations." *Journal of Computational Physics.* 79: 12-49.

Sutherland, D. R. J., Noble, D. R., Steynor, J., Davey, T. A. D., Bruce, T. 2017. "Characterisation of Current and Turbulence in the FloWave Ocean Energy Research Facility." *Ocean Engineering.* 139: 103115.

Sutherland, D., Stephanie, O. S., Michael, B., Ian, M., Jeffrey, S., Thomas, D., Tom, B. 2017. "Experimental optimisation of power for large arrays of cross-flow tidal turbines." *Renewable Energy.* 116. 10.1016/j.renene.2017.10.011.

Taniguchi, N., Kaneko, A., Yuan, Y., Gohda, N., Chen, H., Liao, G., Yang, C., Minamidate, M., Adityawarman, Y., Zhu, X.-H., Lin ,J. 2010. "Long-term acoustic tomography measurement of ocean currents at the northern part of the Luzon Strait." *Geophys. Res. Lett.* 37: L07601.

Wen, H., Bing, R. 2018. "A non-reflective spectral wave maker for SPH modeling of nonlinear wave motion." *Wave Motion.* 79: 112-128.

Wendland, H. 1995. "Piecewiese polynomial, positive definite and compactly supported radial functions of minimal degree." *Advances in Computational Mathematics.* 4: 389-396.

Xu, R, Stansby, P., Laurence, D. 2009. "Accuracy and stability in incompressible SPH (ISPH) based on the projection method and a new approach." *Journal of Computational Physics.* 228(18): 6703-6725.

Yabe, T., Xiao, F., Utsumi, T. 2001. "The Constrained Interpolation Profile Method for Multiphase Analysis." *Journal of Computational Physics.* 169: 556-593.

Zhang, A., Sun, P., Ming, F., Colagrossi, A. 2017. "Smoothed particle hydrodynamics and its applications in fluid-structure interactions." *Journal of hydrodynamics.* 29(2): 187-216.